PERIODICO di MINERALOGIA
established in 1930

Dipartimento di Scienze della Terra
Sapienza Università di Roma

An International Journal of
Mineralogy, Crystallography, Geochemistry,
Ore Deposits, Petrology, Volcanology
and applied topics on Environment, Archaeometry and Cultural Heritage

Cytotoxic and pro-inflammatory early effects of mineral fibres on human alveolar epithelial and immune cells

Anna Maria Bassi [1,6], Serena Mirata [1,6], Vanessa Almonti [1,6], Sara Tirendi [1,6], Stefania Vernazza [1,6], Laura Fornasini [2], Simona Raneri [3], Danilo Bersani [2], Mario Passalacqua [1], Alessandro F. Gualtieri [4], Sonia Scarfì [5,6]

[1] Department Experimental Medicine, University of Genova, Via L. Alberti 2, 16132, Italy
[2] Department of Mathematical, Physical and Computer Sciences, University of Parma, Parco Area delle Scienze 7/A, 43124 Parma, Italy
[3] ICCOM-CNR - Institute of Chemistry of OrganoMetallic Compounds, National Research Council, Via G. Moruzzi 1, 56124 Pisa, Italy
[4] Department of Chemical and Geological Sciences, University of Modena and Reggio Emilia, Via G. Campi 103, I-41125 Modena, Italy
[5] Department Earth, Environment and Life Sciences, University of Genova, Corso Europa 26, 16132, Italy
[6] Inter-University Center for the Promotion of the 3Rs Principles in Teaching & Research (Centro 3R), Italy

ARTICLE INFO

Submitted: May 2023
Accepted: July 2023
Available on line: July 2023

* Corresponding author:
serena.mirata@edu.unige.it

Doi: 10.13133/2239-1002/18082

How to cite this article:
Bassi A.M.et al. (2023)
Period. Mineral. 92, 223-239

ABSTRACT

When interacting with macrophages and epithelial lung cells, inhaled harmful particles trigger the pro-inflammatory process which, in turn, promotes the recruitment of circulating monocytes at the site of injury and their subsequent differentiation towards a macrophage phenotype. In this study, we evaluated the early cytotoxic and pro-inflammatory effect of three well-known carcinogenic fibres (i.e., crocidolite, chrysotile and erionite) on human THP-1 naïve monocytes and A549 alveolar epithelial cells, mimicking the recruitment and engagement of circulating monocytes at the site of fibre deposition. In both cell lines, all fibres showed significant direct cytotoxicity, with crocidolite and chrysotile inducing a higher time-dependent increase of the oxidative stress respect to erionite. Moreover, the direct exposure to the three fibres prompted the activation of THP-1 naïve monocytes towards the M0 pro-inflammatory phenotype, upregulating the gene expression of differentiation markers and promoting the release of pro-inflammatory cytokines. Finally, we evaluated the differentiation and activation of THP-1 naïve cells in response to conditioned media from fibre-treated A549 alveolar epithelial cells and M0-THP-1 macrophages. Interestingly, the exposure to chrysotile-treated media promoted the highest upregulation of pro-inflammatory mediators, suggesting that the soluble factors secreted in response to this fibre cause a stronger recruitment and activation of naïve monocytes.

Keywords: asbestos; inflammation; acute toxicity; naïve immune cells.

INTRODUCTION

Asbestos-related diseases are an important cause of mortality for at-risk workers, as well as for people living near asbestos mines or buildings with open sources of airborne contamination (O'Reilly et al., 2007). The group of asbestos fibres includes six mineral species: chrysotile, the only serpentine one, and five fibrous amphiboles, which are amosite, crocidolite, asbestos anthophyllite, asbestos tremolite and asbestos actinolite (Gualtieri, 2023). An asbestiform habit is also displayed by fibrous erionite, which can occur in three different forms based on the most abundant extra-framework cation, i.e., erionite-

Na, erionite-K, and erionite-Ca (Mattioli et al., 2016; Ballirano et al., 2017). Erionite is mainly considered an environmental contaminant since its airborne presence has been linked to the outbreak of malignant mesothelioma epidemics in several areas of the world (Dikensoy, 2008; Giordani et al., 2017).

In 2012, the International Agency for Research on Cancer (IARC) classified crocidolite, chrysotile, and fibrous erionite as carcinogenic substances for humans (Group 1) due to their well-known toxicity related to their chemical-physical characteristics (i.e., morphology, surface activity, biodurability and iron content) (IARC, 2012). As it has been widely demonstrated in recent years, the biodurability of mineral fibres (i.e., their resistance to chemical/biochemical alterations) plays a key role in determining the severity of their cytotoxic and genotoxic effects leading to the onset of asbestos-related diseases (Barlow et al., 2017; Gualtieri et al., 2018; Gualtieri et al., 2019; Gualtieri, 2021; Madl and O'Neill, 2023). For this reason, chrysotile is the only asbestos/asbestiform fibre still used and mined worldwide in several countries claiming its safe use due to its low biodurability. This characteristic is supposed to make it allegedly less toxic than the amphibole minerals (Egilman and Howe, 2007; Baur and Frank, 2021). In addition, the World Health Organization (WHO) still encounters difficulties in the definition of the minimum threshold rate of asbestos fibres inhalation leading to toxic effects due to the long latency period leading to the onset of chronic lung diseases (i.e., lung cancer and malignant mesothelioma). Since the toxicity of mineral fibres is still an open issue in the biomedical research field, a more in-depth understanding of the molecular mechanisms underlying the early and long-term interactions between particulate matter and living cells could ultimately contribute to the identification of novel strategies for the prevention and treatment of such lethal pathologies.

In the early stages, i.e., once inhaled, mineral fibres settle into the interstitial spaces of the respiratory tract and interact with alveolar macrophages and epithelial lung cells, triggering an acute lung inflammatory process, which during time, and mainly due to the biodurability of the fibres, becomes a chronic condition leading to fibrosis and scarring of the tissue with consequent loss of functionality, respiratory failure and, possibly, tumour formation (Yu et al., 2019). In addition to tissue-resident alveolar macrophages, the involvement of newly differentiated macrophages during the inflammatory process can also result from the recruitment of circulating monocytes by chemotactic factors, further exacerbating and propagating the frustrated immune response (Guilliams et al., 2018). In this regard, the human monocyte-like cell line THP-1 represents a valuable model to investigate the initiation of the inflammatory process induced by harmful stimuli, since these cells can recapitulate *in vitro* the physiological differentiation towards the M0 activated macrophage phenotype when triggered by inflammatory agents (Epelman et al., 2014; Bosshart and Heinzelmann, 2016).

Therefore, the present study aimed at investigating the early pro-inflammatory and cytotoxic effects promoted by direct contact of human THP-1 naïve monocytes and A549 alveolar epithelial cells to crocidolite, chrysotile and erionite mineral fibres, mimicking the stage of cell recruitment and engagement of circulating monocytes at the site of fibre deposition in the lung. Considering that circulating monocytic cells are mainly activated by soluble mediators (i.e, cytokines and chemokines) released into the extracellular environment when the surrounding cells encounter harmful stimuli, we also investigated the stimulation of THP-1 cells differentiation and activation to a pro-inflammatory M0 phenotype by use of conditioned media from A549 alveolar cells or THP-1-M0 already differentiated macrophages challenged with the mineral fibres for 24 h. Firstly, we quantified the early direct effect of the three mineral fibres on the viability index of both cell lines, as well as on the induction of oxidative stress by means of Reactive Oxygen Species (ROS) production. Then, the gene expression levels of macrophage differentiation markers and pro-inflammatory mediators was evaluated on naïve THP-1 monocytes after 24 h of direct treatment with the mineral fibres. Finally, the gene expression profile of naïve THP-1 cells was assessed after incubation with conditioned media obtained from fibre-exposed A549 cells or THP-1-M0 macrophages to verify whether the pro-inflammatory soluble mediators released by these fibre-treated cells could induce phenotypical changes in THP-1 naïve monocytes, promoting their maturation towards the M0 macrophage phenotype.

MATERIALS AND METHODS

Mineral fibres

The present study was focused on the following mineral fibres:

- UICC standard crocidolite (South Africa, NB #4173-111-3) with chemical formula formula $(Na_{1.96}Ca_{0.03}K_{0.01})_2(Fe^{2+}_{2.34}Fe^{3+}_{2.05}Mg_{0.52})_{4.91}(Si_{7.84}Al_{0.02})_{7.86}O_{21.4}(OH)_{2.64}$. Sample contains minor impurities of hematite, magnetite, and quartz. Complete characterisation of the sample is available in Gualtieri et al. (2018) and Pacella et al. (2019).

- Chrysotile from Balangero (Turin, Italy) with chemical formula $(Mg_{5.81}Fe^{2+}_{0.15}Al_{0.27}Fe^{3+}_{0.09}Cr_{0.01})_{6.33}Si_{3.97}O_{10}(OH)_{7.11}$. Sample contains minor impurities of antigorite, balangeroite, calcite, clinochlore, diopside, dolomite, magnetite, microcline, plagioclase, talc. Complete characterisation of the sample is available in Pollastri et

al. (2016) and Gualtieri et al. (2018).

- Fibrous erionite-Na from Jersey (Nevada, USA) with chemical formula $[(Na_{5.35}K_{2.19}Ca_{0.15}Mg_{0.11}Ti_{0.05})_{7.85}(Si_{28.01}Al_{7.90})_{35.91}O_{72}{\cdot}28.13H_2O]$ with traces of clinoptilolite. Complete characterisation of the sample is available in Gualtieri et al. (2016) and Pollastri et al. (2016).

To prepare the fibre stock solutions, mineral fibres were sterilized by autoclave standard treatment (120 °C for 20 min) and then suspended in phosphate buffered saline (PBS) at the concentration of 5 mg/mL, before sonication for 5 min at 50 Hz with a UP50H Ultrasonic Processor (Hielscher Ultrasonics GmbH, Teltow, Germany) keeping the samples in ice to avoid overheating. Each working solution was then diluted directly in the culture media to obtain the different final concentrations.

Cell cultures

The human monocytic THP-1 cells, obtained from the American Type Culture Collection (LGC Standards srl, Milan, Italy), were cultured in RPMI-1640 (Euroclone, Milan, Italy) supplemented with 10% FBS (Euroclone), 2 mM L-glutamine (Euroclone) and penicillin/streptomycin as antibiotics (Corning Inc, NY, USA). When required, THP-1 monocytes were polarised into non-activated M0 macrophages by adding 20 ng/mL phorbol-12-myristate 13-acetate (PMA, PeproTech EC, London UK) as described in Mirata et al. (2022).

The human epithelial adenocarcinoma lung cell line A549 was obtained from the Interlab Cell Line Collection (IRCCS Ospedale Policlinico San Martino, Genoa, Italy) and cultured in high glucose DMEM (Biowest, Nuaillé, France) supplemented with 10% FBS (Euroclone), 2 mM L-glutamine (Euroclone) and penicillin/streptomycin as antibiotics (Corning Inc). Both cell lines were cultured at 37 °C in a humidified 5% CO_2 atmosphere.

Fibre characterisation

The mineral fibres were investigated by micro-Raman spectroscopy after 24 h incubation with A549 alveolar cells. Cell-fibres slides were prepared as described in Mirata et al. (2022). Micro-Raman measurements were performed with a HORIBA Jobin Yvon LabRam confocal micro-spectrometer (300 mm focal length) and a HORIBA Jobin Yvon LabRam HR Evolution confocal micro-spectrometer (800 mm focal length), with an integrated Olympus microscope with 10x, 50x ULWD and 100x objectives, using a frequency doubled Nd:YAG 473.1 nm and a diode 785 nm laser lines. The system was calibrated with the 520.6 cm^{-1} Raman peak of silicon in the low-wavenumber range (100-1200 cm^{-1}) and with the emission lines of a gas lamp in the high-wavenumber range (3300-3800 cm^{-1}). The spectral resolution is ~4 cm^{-1} with the 473.1 nm line and ~1 cm^{-1} with the 785 nm one. The accumulation time was 60 s with at least 3 repetitions. The fluorescence background was removed by subtracting a polynomial curve as baseline. The Raman signals were deconvoluted with Gaussian-Lorentzian curves to determine the peaks parameters and identify the mineralogical phases.

Cytotoxicity tests

To evaluate the cytotoxic effect of the different types of mineral fibres, THP-1 cells were plated at $25x10^3$ cells/well, while A549 cells were seeded at $10x10^3$ cells/well in 96-well plates. After 24 h, the CRO, CHR and ERI solutions were directly added in culture medium at different concentrations (25 μg/mL, 50 μg/mL and 100 μg/mL final concentrations) and the plates were incubated for 24 and 48 h. At the end of each experimental time, cell viability was measured with the MTT assay (0.5 mg/mL final concentration) as previously reported (Pozzolini et al., 2016). In each experiment, each condition was tested eight times. Results are the mean ± SD of three experiments and are expressed as percentage of viable cells as compared to control cells.

Reactive oxygen species quantification

The intracellular production of ROS induced by the mineral fibres was measured according to De La Fuente et al. (2020). Briefly, THP-1 monocytes were plated at $25x10^3$ cells/well, whereas A549 cells were seeded at $10x10^3$ cells/well in 96-well plates. After 24 h, cells were washed once with Hanks' balanced salt solution (HBSS) and then incubated for 45 min at 37 °C with 10 μM 2',7'-dichloro-dihydro-fluorescein diacetate dye (DCF) in HBSS (Life Technologies, Milan, Italy). After washing with HBSS to remove excess of dye, 100 μg/mL of the three mineral fibres or 200 μM H_2O_2 (positive control) were added to each well in complete medium without phenol red. The fluorescence was recorded by a CLARIOstar® Plus multi-mode microplate reader (BMG Labtech, Ortenberg, Germany) at 37 °C and 5% CO_2 at 485/520 excitation/emission wavelengths every 2 h for an interval of 24 h. In each experiment each condition was tested eight times. Results are the mean ± SD of three experiments and are expressed as percentage of ROS production increase/decrease during time as compared to time=0.

Gene expression analyses

The gene expression profile of pro-inflammatory cytokines and macrophage differentiation markers was evaluated in THP-1 cells after direct exposure to the mineral fibres, as well as after treatment with conditioned media obtained from fibre-treated A549 cells and fibre-treated THP-1-derived M0 macrophages for 24 h. Briefly, for the analysis in direct contact conditions, THP-1

monocytes were seeded in 6-well plates at $5x10^5$ cells/well and then incubated for 24 h in presence or absence of 50 μg/mL CRO, CHR and ERI mineral fibres (direct exposure).

To analyse the effect of the conditioned media, A549 cells and THP-1-M0 macrophages were seeded in 6-well plates at $4x10^5$ and $5x10^5$ cells/well, respectively, and then incubated with 50 μg/mL of the three mineral fibres for 24 h. Then, the conditioned media were collected and centrifuged at maximum speed for 10 min to remove cell debris and fibres, they were filtered with PRIMO 0.22 μm Syringe Filter (Euroclone) and diluted 1:1 with complete culture medium and added to THP-1 naïve monocytes seeded in 6-well plates ($5x10^5$ cells/well) for 24 h.

After fibre direct exposure or conditioned media exposure, THP-1 cells were retrieved to extract total RNA. Total RNA was extracted using the NucleoSpin RNA, Mini kit (MACHEREY-NAGEL, Dueren, Germany) according to the manufacturer's instructions. The quality and quantity of RNA were analyzed using a NanoDrop spectrophotometer (Nanodrop Technologies, Wilmington, DE, USA). The cDNA was synthesized from 1 μg of RNA by using a cDNA Synthesis Kit (biotechrabbit GmbH, Henningsdorf, Germany). Each PCR reaction was performed in 10 μL containing: 4× master mix (biotechrabbit GmbH), 0.2 μM of each primer and 5 ng of cDNA. All samples were analyzed in triplicate. The following thermal conditions were used: initial denaturation at 95 °C for three minutes, followed by 45 cycles with denaturation at 95 °C for 15 s, and annealing and elongation at 60 °C for 60 s. The fluorescence was measured at the end of each elongation step. For all experimental conditions, the gene expression profile of interleukin-1β (IL-1β), interleukin-6 (IL-6), interleukin-8 (IL-8), monocyte chemoattractant protein-1 (MCP-1), tumour necrosis factor-α (TNF-α), scavenger receptor CD163 (CD163) and C-X-C motif chemokine ligand-10 (CXCL10) was evaluated by qPCR relative to untreated THP-1 cells. Values were normalized to the HPRT-1 housekeeping gene mRNA expression. All primers (Table 1) were designed using the Beacon Designer 7.0 software (Premier Biosoft International, Palo Alto, CA, USA) and obtained from TibMolBiol (Genoa, Italy). Data analyses were obtained using the DNA Engine Opticon® 3 Real-Time Detection System Software program (3.03 version), and to calculate the relative gene expression compared to the untreated control sample, the comparative threshold Ct method was used (Vandesompele et al., 2002) with the Gene Expression Analysis for iCycler iQ™ Real Time Detection System software (Bio-Rad, Milan, Italy). Experiments were performed thrice in triplicate.

Pro-inflammatory cytokine release

THP-1 cells were seeded in 24-well plates at $1x10^5$ cells/well and incubated with CRO, CHR and ERI (50 μg/mL final concentration) in RPMI complete medium for 24 h. Then, each cell suspension was transferred into collecting tubes, centrifuged at 500 x *g* for 10 min and filtered with PRIMO 0.22 μm Syringe Filters (Euroclone), before storage at -20 °C until further use. The release of IL-1β and TNF-α in the collected cell media was quantified by ELISA kits, namely Human IL-1beta ELISA Kit (detection range between 15.6 pg/mL and 500 pg/mL) and TNF-alpha Human ELISA Kit (detection range between 15.63 pg/mL and 1000 pg/mL), following the manufacturer's instructions (Abcam, Cambridge, UK).

Statistical analyses

Statistical analysis was performed using one-way ANOVA plus Tukey's post-test (GraphPad Software, Inc., San Diego, CA, USA). Results with p values <0.05 were considered significant.

Table 1. List of primer pairs used for qPCR experiments in human naïve THP-1 monocytes.

GENE	GenBank (a.n.)	Forward	Reverse	Size (bp)
IL-1β	NM_000576.3	TGATGGCTTATTACAGTGGCAATG	GTAGTGGTGGTCGGAGATTCG	140
IL-6	NM_001318095.2	CAGATTTGAGAGTAGTGAGGAAC	CGCAGAATGAGATGAGTTGTC	194
IL-8	NM_000584.4	AATTCATTCTCTGTGGTATC	CCAGGAATCTTGTATTGC	127
TNF-α	NM_000594.4	GTGAGGAGGACGAACATC	GAGCCAGAAGAGGTTGAG	113
MCP-1	NM_002982	CTTCTGTGCCTGCTGCTC	CTTGCTGCTGGTGATTCTTC	156
CD163	NM_004244.5	GTCGCTCATCCCGTCAGTCATC	GCCGCTGTCTCTGTCTTCGC	114
CXCL10	NM_001565.4	GAAAGCAGTTAGCAAGGAAAGGTC	ATGTAGGGAAGTGATGGGAGAGG	120
HPRT-1	NM_000194.3	GGTCAGGCAGTATAATCCAAAG	TTCATTATAGTCAAGGGCATATCC	144

RESULTS

Raman Fibre Characterisation

After incubation with A549 alveolar cells, the mineral fibres deposited on cells were directly investigated by micro-Raman spectroscopy in the resulting cell-fibre systems. Indeed, the three mineral fibres detected into and onto the cells showed different morphologies, consisting of curvilinear fibres for chrysotile, thin and rigid fibres for crocidolite and shorter fibres for erionite, as observed by Mirata et al. (2022). Each type of mineral fibre was identified by its distinctive Raman spectrum (Figure 1). In the low-wavenumber spectral range (Figure 1A), chrysotile signals occur at 130, 236, 391 and 692 cm^{-1}, corresponding to the typical vibrations of the serpentine polymorphs (Petriglieri et al., 2015; Fornasini et al., 2022). Erionite is characterised by the most intense peak at 486 cm^{-1} with a shoulder at ~468 cm^{-1} and a less intense band at ~340 cm^{-1} (Croce et al., 2013; Tsai et al., 2021). Crocidolite shows the main peaks at 145, 164, 199, 297, 372 (with a shoulder at ~360), 538, 574, 663 and 967 cm^{-1} (Croce et al., 2013; Rinaudo et al., 2004).While erionite and crocidolite were confidently recognized by their peculiar signals in the low-wavenumber spectral range, the identification of chrysotile was confirmed by its typical Raman bands of the OH stretching vibrations, in order to unequivocally distinguish its signature among those of the other serpentine polymorphs (Figure 1B). Chrysotile shows the main peak at 3696 cm^{-1} with a shoulder at ~3685 cm^{-1} and a lower intense band at ~3645 cm^{-1} (Petriglieri et al., 2015; Fornasini et al., 2022).

Cytotoxicity in epithelial alveolar cells and naïve monocytes

The potential acute cytotoxicity of the three mineral fibres was evaluated on A549 and THP-1 naïve cells after 24 and 48 h exposure to increasing concentrations of CRO, CHR, and ERI, by the MTT test. Adherent A549 alveolar epithelial cells in direct contact with the three fibres showed the highest mortality rate, with the lowest dose tested (25 μg/mL) already showing a ≈50% cell death for CRO and ERI with no significant differences between 24 and 48 h incubation (Figure 2, black and white bars, respectively). At the higher concentrations tested (50 and 100 μg/mL) CRO and ERI induced a slight increase in cell death at both experimental times, as compared to the lower concentration of the same fibre. CHR did not show a dose-response behavior, displaying the same mortality rates at 24 and 48 h (40% and 50%, respectively), at the three concentrations tested. In addition, suspensions of THP-1 naïve monocytes in contact with the three mineral fibres added to the cell medium showed a significant, and dose-dependent, mortality rate in presence of CRO and ERI, at both 24 and 48 h exposure times (Figure 3, black and white bars, respectively), while in presence of CHR, THP-1 monocytes showed a slight, dose-independent (13-17%) cell toxicity only in the first 24 h of incubation. Since the MTT cytotoxicity test is based on the assessment of the mitochondrial function, we can ascribe this slight toxic effect of CHR at 24 h to an initial alteration in some mitochondrial function, followed by a recovery after 48 h. The result is that THP-1 monocyte viability is not really affected by CHR. Conversely, CRO and ERI show cytotoxicity MTT indexes that are much more significant

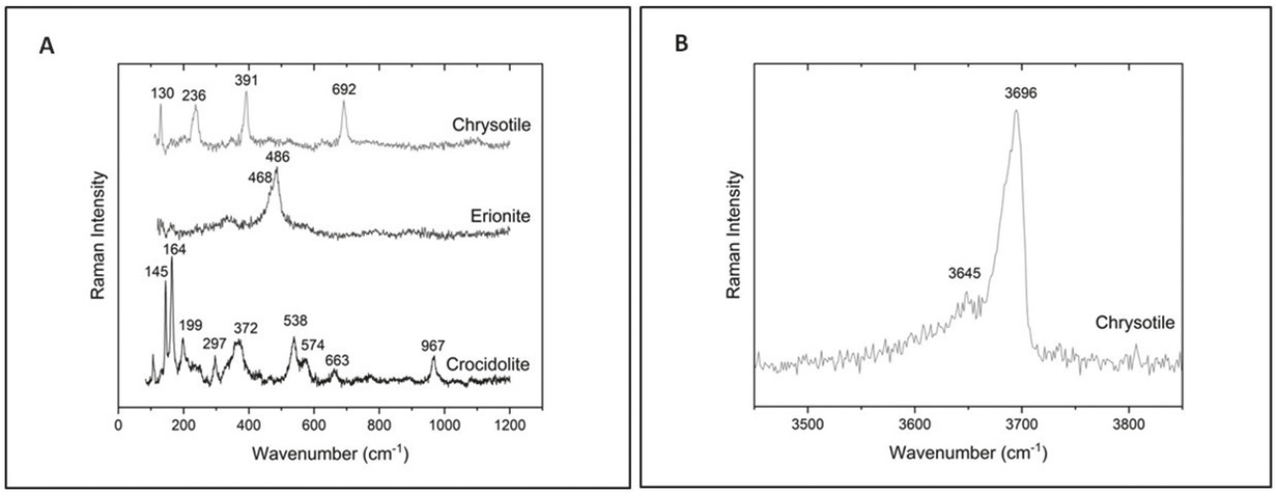

Figure 1. Raman characterisation of the mineral fibres CRO, CHR and ERI. (A) Micro-Raman spectra of the mineral fibres crocidolite, chrysotile and erionite in the low-wavenumber spectral range. (B) Micro-Raman spectrum of chrysotile fibres in the OH-stretching spectral range.

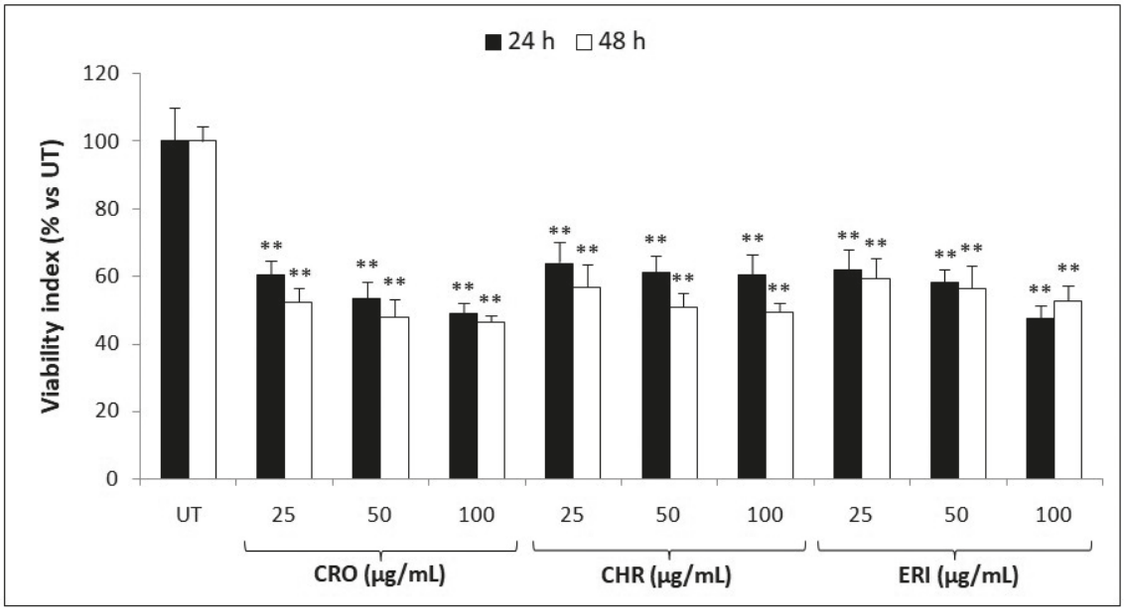

Figure 2. Cell toxicity quantification in A549 epithelial alveolar cells after exposure to mineral fibres. A549 cells cytotoxicity evaluation by the MTT test in the presence of 25, 50 and 100 µg/mL of the mineral fibres CRO, CHR and ERI after exposure for 24 h (black bars) and 48 h (white bars). Results are expressed as cell percentages relative to control cells (UT) and are the mean ± SD of three independent experiments, in which each condition was tested eight times. Asterisks indicate the significance in a paired Tukey test (Tukey vs UT: ** p <0.0001).

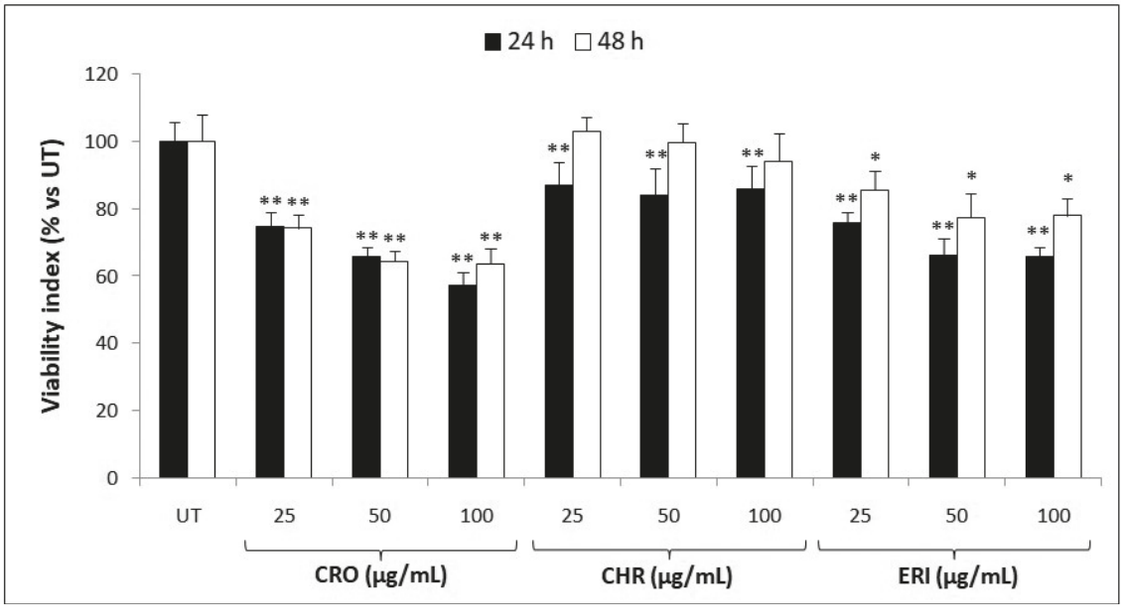

Figure 3. Cell toxicity quantification in naïve THP-1 monocytes after exposure to mineral fibres. Naïve THP-1 monocytes cytotoxicity evaluation by the MTT test in the presence of 25, 50 and 100 µg/mL of the mineral fibres CRO, CHR and ERI after exposure for 24 h (black bars) and 48 h (white bars). Results are expressed as cell percentages relative to control cells (UT) and are the mean ± SD of three independent experiments, in which each condition was tested eight times. Asterisks indicate the significance in a paired Tukey test (Tukey vs UT: * p <0.05, ** p <0.001, respectively).

than CHR at 24 h, and these indexes are maintained also at 48 h, indicating that these fibres, other than altering the mitochondrial function of THP-1 monocytes, are also causing a significant cell death due to the significant and persistent different MTT values compared to the untreated cells.

Oxidative stress

Intracellular ROS levels were measured in A549 alveolar epithelial cells (Figure 4) and THP-1 naïve monocytes (Figure 5) using DCF fluorescent dye-based assay. In particular, intracellular ROS production was recorded every 2 h, for a total of 24 h, following treatment with 200 μM H_2O_2 (positive control) or with 100 μg/mL of mineral fibres. As compared to untreated cells, H_2O_2-treated A549 cells (Figure 4A) showed a significant ROS increase already at time=0 (corresponding to 10 min after addition of the stimulus), reaching a peak of 10-folds after 6 h, before slowly decreasing to basal values after 24 hours. During exposure to the three fibres, the ROS production evidenced a different behaviour as compared to the H_2O_2 positive control. Indeed, starting at time=0 (10 min after fibre administration) ROS levels steadily increased during the 24 h-recording with all the three fibres, reaching different levels of oxidative stress at the end of the incubation. In particular, CRO and CHR induced the highest ROS increase (2.0- and 2.4-folds increase, respectively) compared to the untreated control, while ERI induced the lowest ROS production (1.27-folds increase), as shown in Figure 4 (panels B, C and D, respectively).

In THP-1 naïve monocytes (Figure 5), H_2O_2 treatment led to a significant ROS increase already at time=0 (3.0-folds increase versus untreated control, panel A) reaching a peak after 6 h, followed by a slow decrease till the end of experimental conditions (24 h). Conversely, during exposure to the three fibres, THP-1 cells showed a time-dependent significant ROS increase compared to control cells, reaching a plateau after 20-22 h incubation especially during CRO and CHR fibre treatments (11.1- and 18.5-folds increase, panels B and C, respectively, compared to the untreated control). ERI-treated THP-1, like A549 cells, showed lower oxidative stress levels than CRO- and CHR-treated cells, reaching a maximum of 1.5-folds increase compared to control cells at 24 h (panel D).

THP-1 activation

The activation of THP-1 naïve monocytes was evaluated by measuring macrophage differentiation

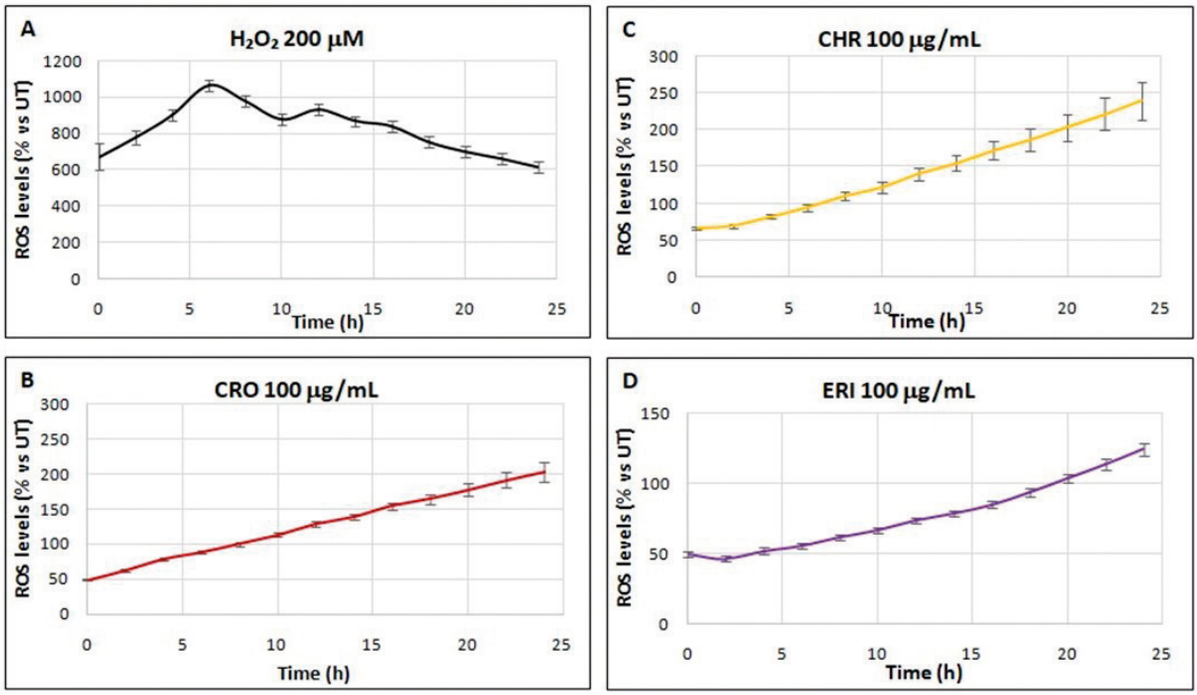

Figure 4. Intracellular ROS production measured by DCF fluorometric analysis in A549 cells incubated for 24 h with 100 μg/mL of crocidolite (panel B), chrysotile (panel C) and fibrous erionite (panel D). Cells stimulated with 200 μM H_2O_2 (panel A) are the positive control. Results are expressed as percentages of ROS production compared to the untreated control (UT) and are the mean ± SD of three experiments, in which each condition was tested eight times.

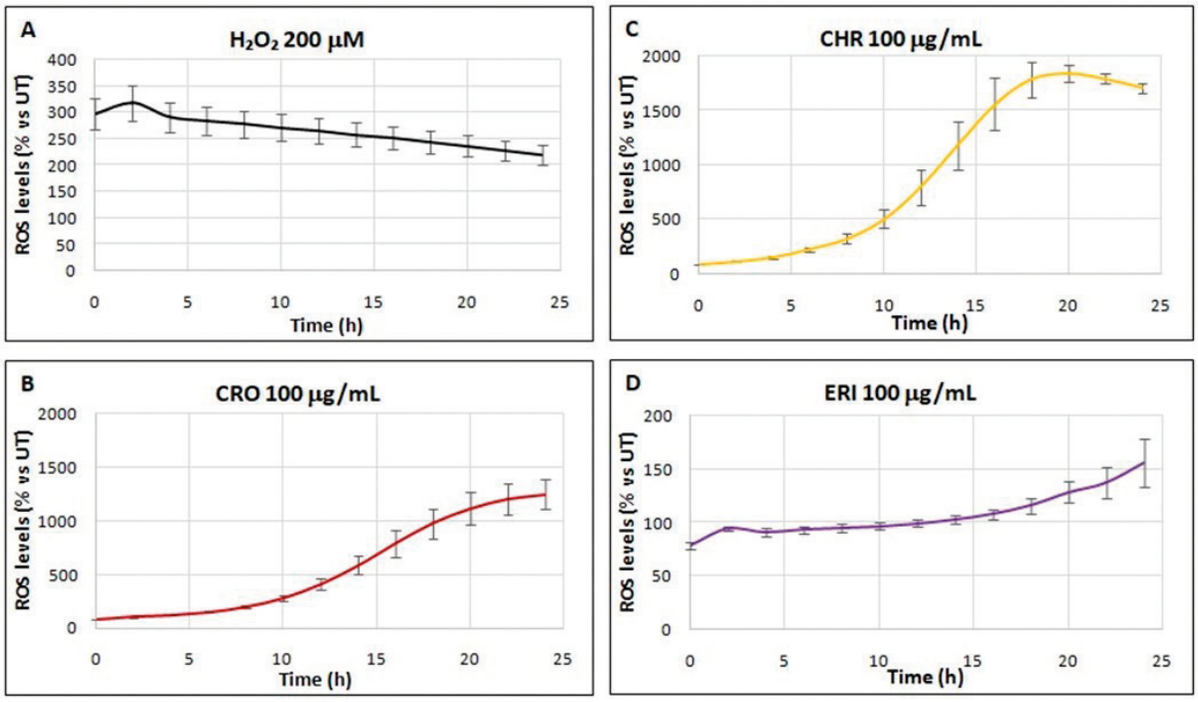

Figure 5. Intracellular ROS production measured by DCF fluorometric analysis in naïve THP-1 monocytes incubated for 24 h with 100 µg/mL of crocidolite (panel B), chrysotile (panel C) and fibrous erionite (panel D). Cells stimulated with 200 µM H_2O_2 (panel A) are the positive control. Results are expressed as percentages of ROS production compared to the untreated control (UT) and are the mean ± SD of three experiments, in which each condition was tested eight times.

marker gene expression as well as pro-inflammatory cytokine gene expression and protein levels, after 24 h exposure to the three mineral fibres. The gene expression of CD163 and CXCL10, which are commonly considered specific markers of monocyte differentiation towards the M0 macrophage phenotype (Littlefield et al., 2014), was evaluated in THP-1 cells following their direct exposure to the three mineral fibres (Figure 6A). After 24 h treatment, CRO and CHR were able to induce a 2-fold increase of CD163 mRNA, while ERI induced a 1.5-fold increase compared to control cells, suggesting an early activation of THP-1 monocytes towards a M0 pro-inflammatory macrophage phenotype after fibre contact. At the same experimental exposure time, early pro-inflammatory IL-1β, IL-6, IL-8, TNF-α cytokine and MCP-1 chemokine gene expressions were evaluated by measuring the mRNA levels of each gene. As reported in Figure 6B, IL-1β mRNA did not show any significant variation as compared to control cells (panel B, blue bars), while TNF-α mRNA showed a decrease after treatment with the three fibres (panel B, yellow bars). Conversely, IL-8, IL-6 and MCP-1 mRNA levels were significantly increased by the 24 h fibre treatment, although to a different extent. In particular, by the comparison with the basal level in the control, IL-8 mRNA resulted in a ≈2- and ≈1.8-folds increase only after CHR and ERI treatment, respectively (panel B, grey bars), while IL-6 increased after CRO (≈2.5-folds) and CHR (≈7.8-folds) treatments (panel C, orange bars), and MCP-1 mRNA increased only during CHR exposure (≈4-folds, blue bars). Furthermore, the protein levels of IL-1β and TNF-α were measured into the cell media after 24 h of exposure to the mineral fibres (Figure 7), since these chemokines are rapidly released by immune cells in response to harmful stimuli, thus promoting the instauration of a pro-inflammatory microenvironment which may ultimately contribute to the insurgence of acute pulmonary inflammation (Zelová and Hošek, 2013; Dinarello, 2018). Indeed, all the three fibres induced a significant increase of IL-1β release as compared to untreated cells (4.1-, 6.4- and 3.4-folds increase for CRO, CHR and ERI, respectively), while only CRO and ERI stimulated a significant release of TNF-α in the extracellular medium after 24 h (panel B, ≈1.6-folds for both vs UT). Overall, these data suggest that the ranking of the pro-inflammatory potential of the three fibres in THP-1 naïve monocytes is: CHR>>CRO>ERI.

Monocytes are circulating cells and more frequently, other than being directly activated by a harmful stimulus, are recruited by chemotactic signals from inflamed tissues leading to extravasation and differentiation

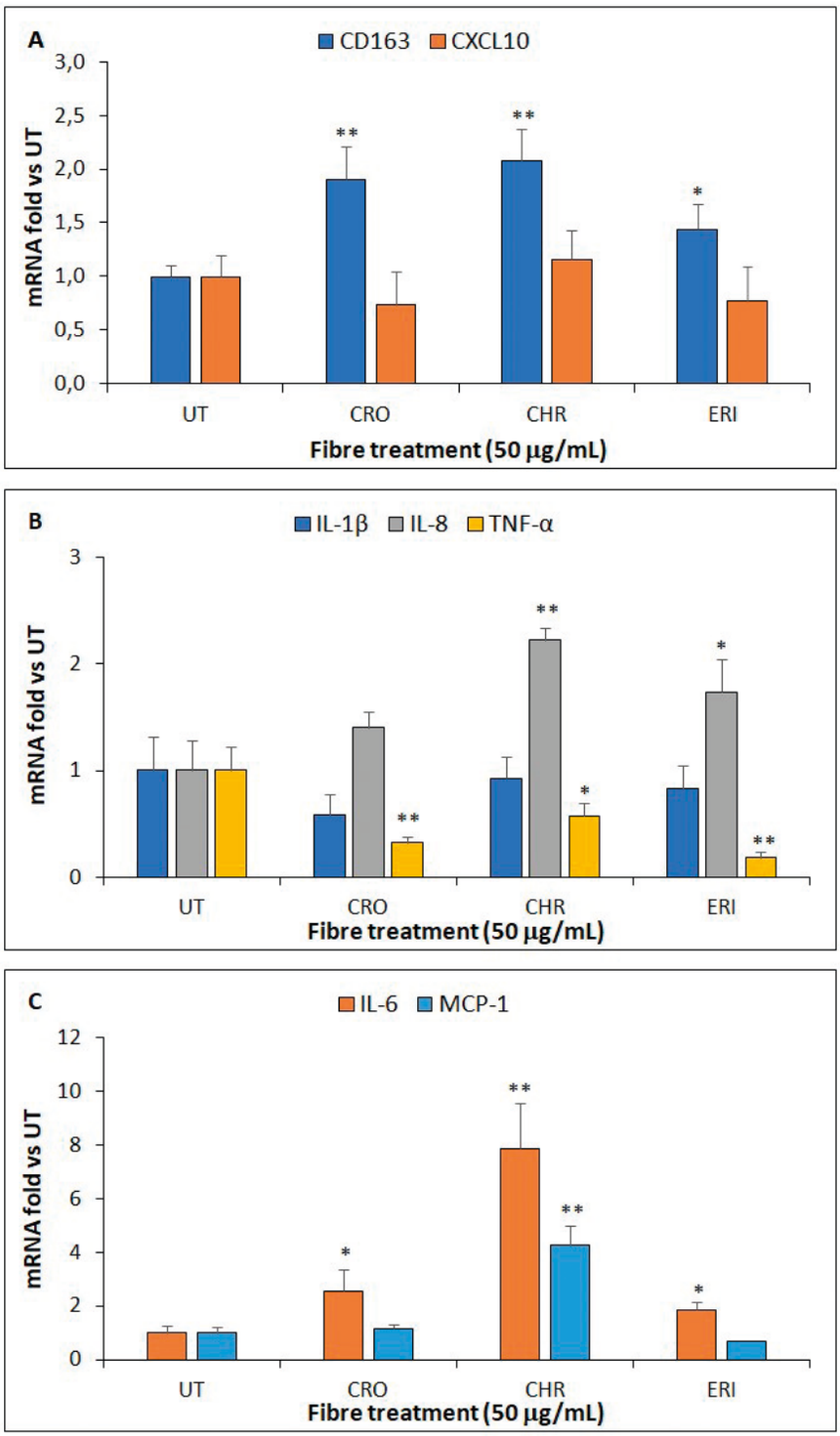

Figure 6. Gene expression profile of naïve THP-1 monocytes treated with mineral fibres. (A) Gene expression of CD163 and CXCL10 measured by qPCR analysis after naïve THP-1 cell incubation for 24 h with 50 µg/mL mineral fibres (CRO, CHR and ERI). Data are normalised to the HPRT-1 housekeeping gene and expressed as mRNA fold increase compared to untreated (UT) THP-1 monocytes. Results are the mean ± SD of three experiments performed in triplicate. Asterisks indicate significance in Tukey test (Tukey vs UT * p <0.05, ** p <0.01, respectively). (B) Gene expression of IL-1β, IL-8 and TNF-α measured by qPCR analysis in naïve THP-1 cells in the same conditions as (A). Tukey vs UT * p <0.05, ** p <0.01, respectively. (C) Gene expression of IL-6 and MCP-1 measured by qPCR analysis in naïve THP-1 cells in the same conditions as (A). Tukey vs UT * p <0.05, **p <0.005, respectively.

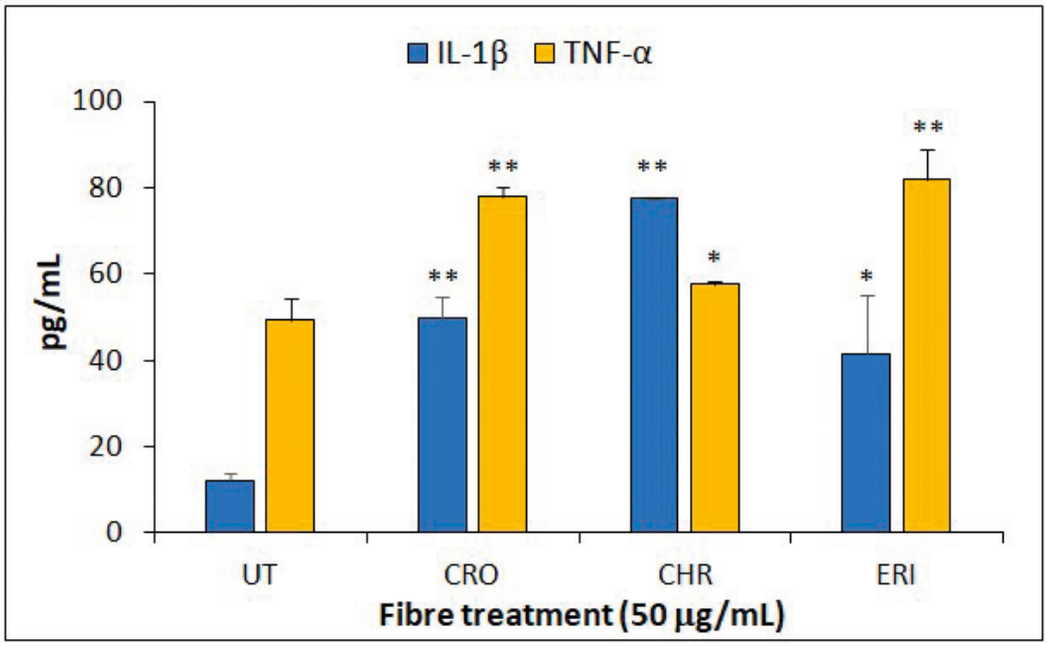

Figure 7. Extracellular release of pro-inflammatory cytokines. IL-1β and TNF-α release (in pg/mL) quantified by ELISA kit in naïve THP-1 monocytes incubated for 24 h with 50 µg/mL of the mineral fibres CRO, CHR and ERI. Results are the mean ± SD of two independent experiments performed in duplicate. Asterisks indicate significance in Tukey test (Tukey vs. UT, * p <0.05, ** p <0.005, respectively).

towards a macrophage phenotype contributing to the exacerbation of the onsite inflammation. Thus, we analysed gene expression variations of indirect fibre stimulation by incubating THP-1 naïve monocytes with 24 h-conditioned media from fibre-treated A549 alveolar cells as well as differentiated THP-1-M0 macrophages (Figures 8 and 9, respectively). The conditioned media from CRO- and ERI-treated A549 strongly stimulated the expression of CD163 and CXCL10 M0 differentiation markers (Figure 8A), while CHR-treated A549 media only increased CXCL10 mRNA expression compared to control cells. Regarding the gene expression profile of pro-inflammatory cytokines, the conditioned media from CHR-treated A549 cells induced a significant increase of IL-6 (panel B, orange bar) and TNF-α (panel C, yellow bar). Conversely, in THP-1 monocytes challenged with the three conditioned media of fibre-treated A549 cells, the mRNA levels of IL-1β, IL-8 and MCP-1 remained unchanged in comparison to naïve monocytes treated with the supernatant of untreated A549 cells.

The effect of the exposure to conditioned media from fibre-treated THP-1-M0 macrophages on THP-1 undifferentiated cells was also evaluated, to verify the ability of already engaged macrophages to recruit and activate naïve monocytes to the site of inflammation. Indeed, the fibre-treated-M0-conditioned media acted as powerful pro-inflammatory stimuli for THP-1 naïve monocytes. In particular, CD163 and CXCL10 M0-differentiation markers were increased in THP-1 naïve cells after treatment with the three conditioned media, compared to control cells (Figure 9A). Also in this case CHR exerted a higher effect than CRO and ERI. Finally, for what concerns the cytokine mRNA overexpression in presence of THP-1-M0 conditioned media, CHR-treatment derived medium was able to significantly increase the production of all investigated mRNAs (IL-1β, IL-8 in panel B and IL-6, TNF-α and MCP-1 in panel C, respectively), while CRO-treatment derived medium only increased IL-1β, IL-8 and IL-6 (panels B and C, respectively), and ERI derived medium led to overexpression of IL-1β, IL-8, IL-6 and MCP-1. In all investigated cytokine gene expressions, CRO- and ERI-derived media evidenced a lower pro-inflammatory potential than CHR-derived medium.

According to our previous findings (Mirata et al., 2022), THP-1 M0 macrophages directly exposed to the three mineral fibres release significant amount of several pro-inflammatory cytokines (i.e., IL-1β, MCP-1 and TNF-α) in the extracellular milieu after only 24 h. In particular, we already observed that CHR promotes the extracellular release of surprisingly high amounts of IL-1β. This cytokine is well-known for promoting the production of other inflammatory mediators (i.e., IL-6, IL-8, MCP-1, COX2, MKP-1) by transcriptional and

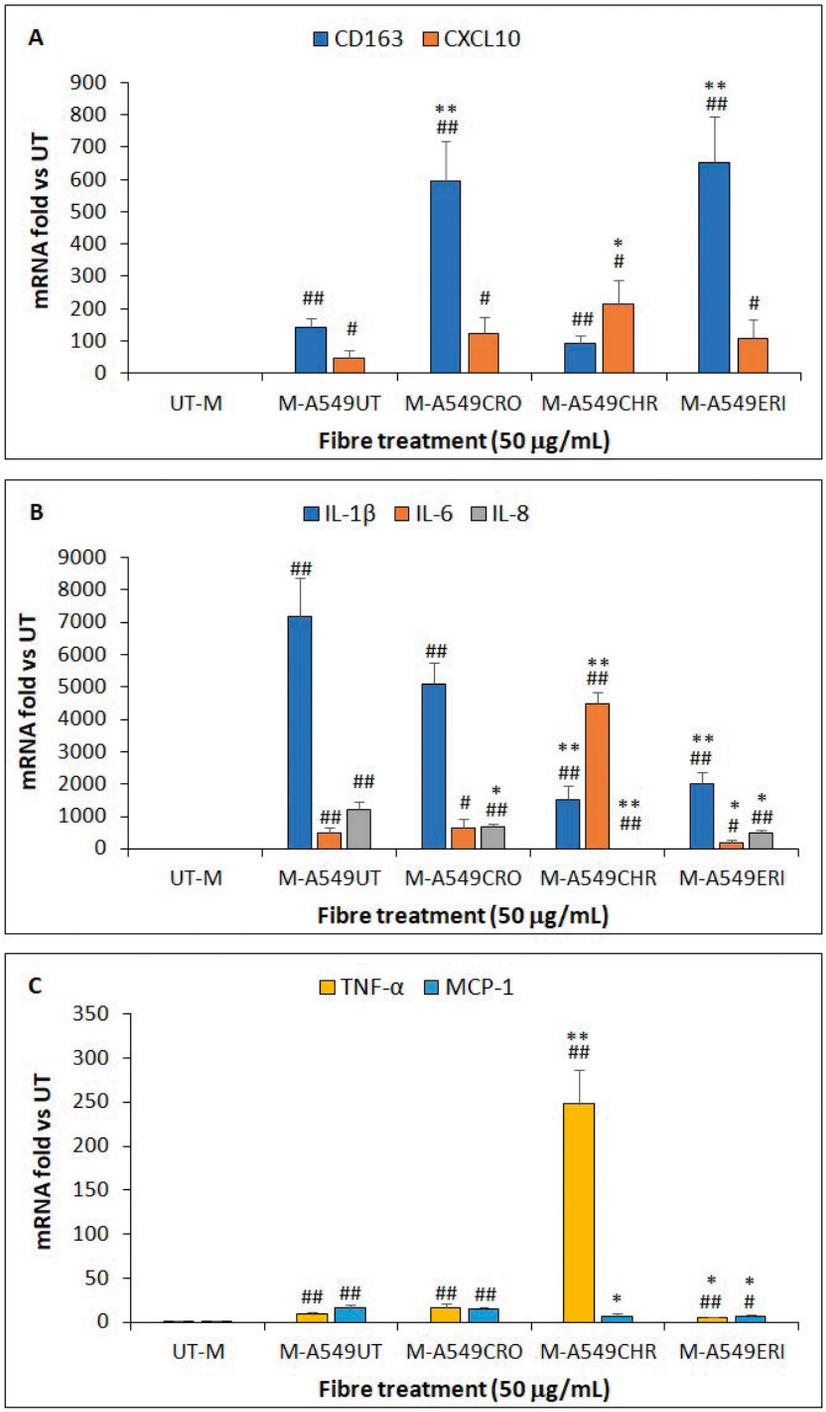

Figure 8. Gene expression profile of naïve THP-1 monocytes exposed to the conditioned media of fibre-treated A549 cells. (A) Gene expression of CD163 and CXCL10 measured by qPCR analysis after naïve THP-1 cell incubation for 24 h with the conditioned media obtained from A549 cells exposed to 50 µg/mL mineral fibres (CRO, CHR and ERI). Data are normalised to the HPRT-1 housekeeping gene and expressed as mRNA fold increase compared to untreated (UT) THP-1 monocytes. Results are the mean ± SD of three experiments performed in triplicate. Asterisks indicate significance in Tukey test (Tukey vs. UT-M # p <0.05, ## p <0.005; Tukey vs M-A549UT * p <0.05, ** p <0.005, respectively). (B) Gene expression of IL-1β, IL-6 and IL-8 measured by qPCR analysis in naïve THP-1 cells in the same conditions as (A). Tukey vs UT-M # p <0.05, ## p <0.005; Tukey vs M-A549UT * p <0.05, ** p <0.005, respectively. (**C**) Gene expression of TNF-α and MCP-1 measured by qPCR analysis in naïve THP-1 cells in the same conditions as (A). Tukey vs UT-M # p <0.01, ## p <0.005; Tukey vs M-A549UT * p <0.05, ** p <0.0005, respectively.

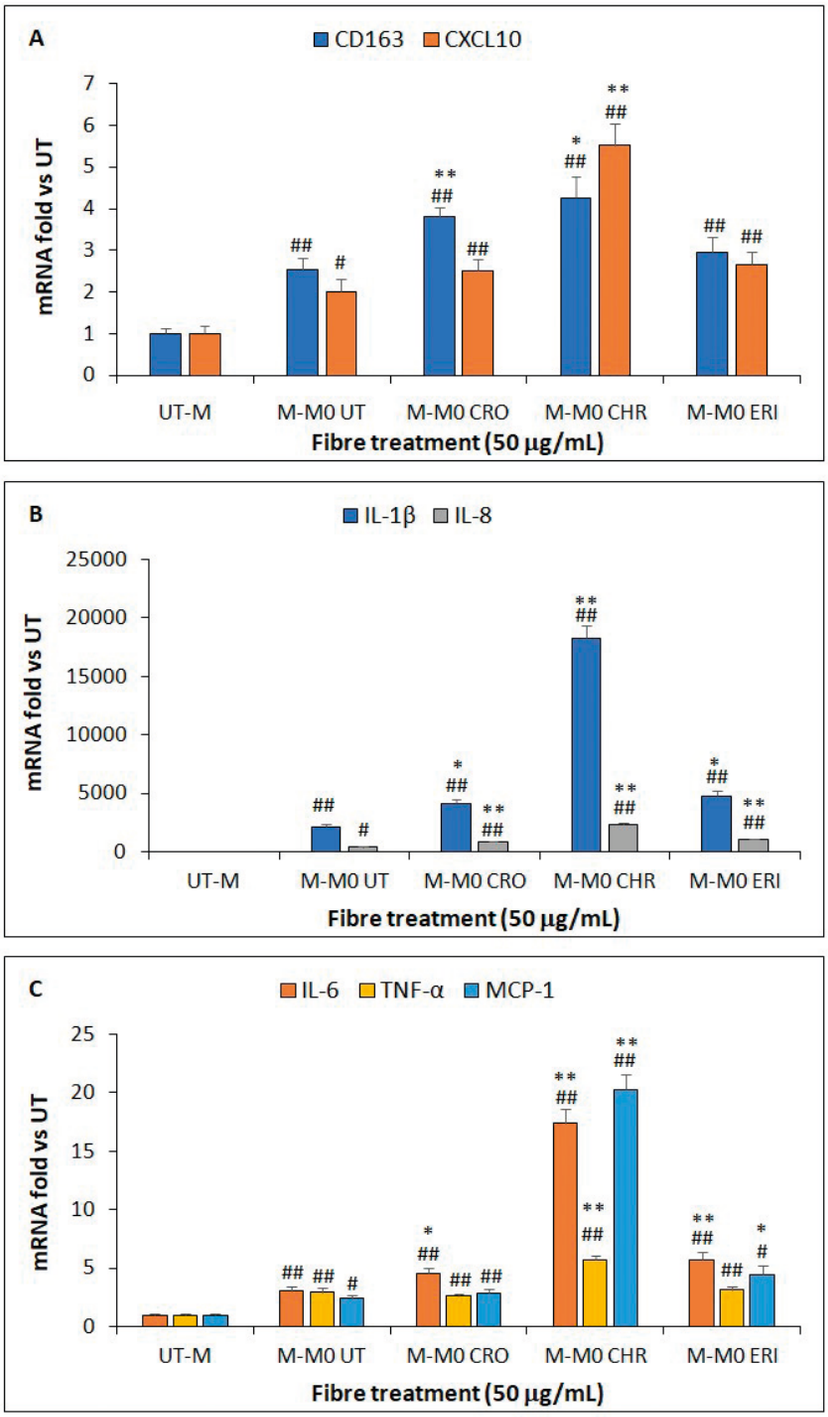

Figure 9. Gene expression profile of naïve THP-1 monocytes exposed to the conditioned media of fibre-treated THP-1-M0 cells. (A) Gene expression of CD163 and CXCL10 measured by qPCR analysis after naïve THP-1 cell incubation for 24 h with the conditioned media obtained from THP-1-M0 cells exposed to 50 µg/mL mineral fibres (CRO, CHR and ERI). Data are normalised to the HPRT-1 housekeeping gene and expressed as mRNA fold increase compared to untreated (UT) THP-1 monocytes. Results are the mean ± SD of three experiments performed in triplicate. Asterisks indicate significance in Tukey test (Tukey vs UT-M # p <0.05, ## p <0.005; Tukey vs M-M0 UT * p <0.01, ** p <0.005, respectively). (B) Gene expression of IL-1β and IL-8 measured by qPCR analysis in naïve THP-1 cells in the same conditions as (A). Tukey vs UT-M # p <0.0005, ## p <0.0001; Tukey vs M-M0 UT * p <0.005, ** p <0.0005, respectively. (**C**) Gene expression of IL-6, TNF-α and MCP-1 measured by qPCR analysis in naïve THP-1 cells in the same conditions as (A). Tukey vs UT-M # p <0.005, ## p <0.001; Tukey vs M-M0 UT * p <0.05, ** p <0.005, respectively.

post-transcriptional mechanisms (Weber et al., 2010). This may explain the significant overexpression of pro-inflammatory cytokines in THP-1 naïve monocytes exposed to the conditioned media from CHR-treated M0 macrophages that we observed in the present paper.

DISCUSSION

According to OECD Guidelines TG403, TG436, TG433 and Guidance Document No. 39 (OECD, 2009a, 2009b, 2009c, 2018), the acute inhalation toxicity tests for regulatory purposes are currently performed only in rats and/or mice. A good *in vitro* model should be as close as possible to the *in vivo* situation, to better reproduce the response of the organism. Indeed, *in vivo* approaches often show a low predictability for the potential risk of inhaled compounds in humans. The problem is related to the low translation of animal biomarkers in humans, for the anatomic, as well as physiological differences of the respiratory tract between animal species (Müller et al., 2010). However, to date, there are no *in vitro* models accepted by regulatory agencies as an autonomous substitute for animal inhalation toxicity tests (Movia et al., 2020). In the attempt to obtain relevant and predictive results for humans, the *in vitro* models should be based on human cells, by replicating *in vitro* the physiological microenvironment. For this purpose, we performed our study on human A549 epithelial alveolar cells and THP-1 naïve monocytes, to identify the early cellular events induced by the exposure to chrysotile, crocidolite and erionite as examples of asbestos-like fibres. Furthermore, we tried to assess the responsivity of naïve monocytes towards the mineral fibres in terms of cell differentiation towards a M0 pro-inflammatory macrophage phenotype and of production of important cytokines also by use of conditioned media from fibre treated A549 alveolar epithelial cells and M0 activated macrophages, as well.

Through Raman analysis the identification of the three mineral fibres in cultures of A549 alveolar cells incubated for 24 h with the fibres was successfully obtained (see Figure 1). In the cell-fibre system, the Raman analysis allowed to recognize the three different chrysotile, crocidolite and erionite fibres by the identification of specific peaks, which were clearly detectable also in presence of cells directly taking contact or phagocyting the fibres, thus demonstrating that is possible to characterize the mineral fibres by this type of analysis in *in vitro* cellular systems, and likely also in *in vivo* testing.

The analyses of cell viability evidenced that A549 alveolar cells were more affected by the fibre treatment in the first 48 h of exposure than THP-1 monocytes (Figures 2 and 3). This is probably related to their different function in the lung environment. In fact, while alveolar cells have the main function of lining respiratory epithelia, monocytes are included in the innate immune system and so are more responsive to the external stimuli activating the inflammatory response. As demonstrated through *in chemico* dissolution tests performed by Gualtieri et al. (2019), chrysotile from Balangero mine is less biodurable than amphibole asbestos and fibrous erionite and the consequent release of metals, iron in particular, could explain the viability decrease in the alveolar cells treated with chrysotile comparable to those treated with the other two fibres, which are traditionally considered more harmful (Giordani et al., 2017; Gualtieri et al., 2019; Fornasini et al., 2022). Conversely, THP-1 naïve monocytes were less affected by the three fibres probably due to lower fibre-cell contact resulting from the non-adherent cell suspension of these immune cells in the culture system. Furthermore, of the three fibres, CHR resulted the less toxic for monocytes, differently from the effect on alveolar cells. Thus, we may conclude that a great deal of early toxicity of the fibres comes from direct plasma membrane-fibre contact, as demonstrated by higher susceptibility of A549 adherent cells, and only partially from the metal release in the cellular media of the same fibres.

It is well known that mineral fibres can induce ROS generation with a different extent typical of each fibre. Intracellular ROS act as second messengers playing a key role in activating cellular responses to stress and in triggering cell damage, including loss of membrane homeostasis and DNA breaks (Matés et al., 2008; Zhou et al., 2019). Regarding the oxidative stress status, in our study, A549 alveolar epithelial cells and THP-1 naïve monocytes showed differences in ROS production during a 24 h time lapse exposure to the investigated fibres both in terms of specific cellular responses highlighted by the differences between the two cell lines, and in terms of the fibre chemical-physical characteristics. For what concerns cellular specific responses it is possible to observe that, although both cell lines undergo a significant ROS increase in the 24 h, A549 alveolar cells show a significant lower production as compared to THP-1 monocytes (Figure 4 vs 5, respectively). This is likely because the latter are immune cells able to transform into phagocytic cells by contact with foreign particles and, as such, much more prone to stress induction and cellular activation, which are necessary steps for the maturation towards the macrophage inflammatory phenotype. Furthermore, a different behaviour in ROS increase is observed among the three fibres with crocidolite and chrysotile inducing a significantly higher response as compared to the erionite fibres in both cell types. This can be related to the different metal ion composition of the fibres, as well as to their different biodurability (Gualtieri et al., 2018; Gualtieri et al., 2019). Indeed, the biodurable crocidolite

exhibits a partial dissolution promoting a significant release of iron, which is known to be involved in the direct formation of ROS (Gualtieri, 2021). Conversely, the non biodurable chrysotile undergoes a fast-dissolution, with several redox-active metals already released in the first 24 h of cellular incubation (i.e., Mg, Fe, Cr, Ni and Co, see Mirata et al., 2022), likely explaining the higher ROS production stimulated by this fibre too. On the other hand, the biodurable erionite contains lower amounts of redox-active metals respect to the other two fibres, as evidenced by the intracellular release of only quantifiable amounts of Al (Mirata et al., 2022), thus a lower ROS production by cells in contact with this fibre, is to be expected. Based on the results obtained we can extrapolate that the ranking of ROS stimulating potential in alveolar epithelial and monocyte cells for the three fibres is: chrysotile>crocidolite>>erionite.

In the attempt to understand the contribution of circulating monocytes to the onset, and especially, to the propagation of the lung inflammation caused by the deposited fibres in the alveoli, we studied the THP-1 naïve monocyte tendency to differentiate towards the M0 macrophage phenotype and the expression of pro-inflammatory cytokines by direct and indirect exposure to the three fibres. The indirect exposure was obtained by incubation of the naïve monocytes with conditioned media from A549 alveolar cells or from already differentiated M0 macrophages, both exposed to the mineral fibres for 24 h.

Both types of stimulation led to a significant increase of M0 macrophage differentiation markers, although to a much higher extent in the presence of the conditioned media as compared to the fibre direct exposure (see panels A of Figures 8 and 9 vs 7, respectively). Indeed, this behaviour can be expected, since circulating naïve monocytes, other than being directly activated by harmful stimuli, which is still possible, are particularly receptive to the chemotactic signals received from inflamed tissues, in this case the alveolar cells and the activated macrophages, leading to extravasation and differentiation of these cells in the site of the inflammation. These results confirm the hypothesis that alveolar epithelial cells, as well as M0-polarised THP-1 cells, in presence of an external mineral fibre stressor, like the mineral fibres, can secrete factors able to trigger the activation of naïve circulating monocytes. The gene expression profile of pro-inflammatory cytokines released by the THP-1 monocytes was also affected by both the fibre direct exposure, as well as the treatment with the conditioned media from fibre treated alveolar and macrophage cells. In the direct treatment the most significant responses from THP-1 naïve cells were obtained in the presence of chrysotile, and this was also true for the conditioned media treatment. Thus, despite the lower acute cytotoxic effect shown by chrysotile in THP-1 monocytes as compared to crocidolite and erionite, the ranking of the inflammatory response elicited by the three fibres can be summarised as follows: chrysotile>>crocidolite>erionite. These results also reflect the behaviour already observed in the rate of the oxidative stress caused by direct contact with the fibres. Thus, we can conclude that, in the case of direct engagement with the stressor, the activation of pro-inflammatory pathways in naïve monocytes is proportional to the rate of oxidative stress induced in the same cells. This is also justified by the fact that intracellular ROS are important second messengers for the NF-kb stress signal transcription factor recruitment, which in turn is responsible for most of the monocyte/macrophage inflammatory responses (Iles and Forman, 2002). Furthermore, these results also highlight that the presumption of a lower toxicity of chrysotile, due to its low biodurability, may be wrong since, since one of the most important carcinogenic parameters (Smith et al., 2016), i.e, the inflammatory response elicited by this fibre, is even more prominent than that caused by the widely recognized carcinogen crocidolite, likely having the same final effect in determining the cancer progression in the lung tissues of exposed subjects.

The activation of naïve THP-1 monocytes towards an inflammatory phenotype due to the direct exposure to the three mineral fibres was also evidenced by the increased release in the cell media of IL-1β and TNF-α pro-inflammatory cytokines (Figure 7), which is not reflected by an increase of gene expression at the mRNA level (Figure 6). These results can be ascribed to the fact that early pro-inflammatory cytokines such as IL-1β and TNF-α can already be present as inactive pro-cytokines within immune cells. In fact, these early pro-inflammatory cytokines require two distinct signals for their activation and release. In the case of IL-1β, the first signal can be triggered by various DAMPs (Damage-Associated Molecular Patterns) following Toll-like receptor activation and prompting the *de novo* synthesis of pro-IL-1β that accumulates in the cell cytoplasm as an inactive precursor. When a second signal induces the activation of the inflammasome, the subsequent activation of caspase-1 promotes the cleavage of pro-IL-1β to its mature active form which is rapidly released in the extracellular milieu. The requirement of this second signal for the secretion of IL-1β active form may represent a safe mechanism which ensures that the induction of inflammatory responses occurs only in the presence of strong harmful stimuli (Dinarello, 2018). However, in an aberrant signalling cascade where it is impossible to remove the source of inflammation, like the mineral fibre, the inflammasome pathway acts as a double-edged sword through an imbalance of cytokine release/signalling promoting the

development of chronic diseases which can increase the risk of cancer evolution (Cox, 2018; Leso et al., 2018; Cox, 2019, 2020; Gaudino et al., 2020; Li et al., 2021).

In these last years it was highlighted the role of sterile DAMPs as activators of inflammatory pathways. Indeed, these sterile stressors can derive from endogenous processes (i.e., necrosis, hypoxia, toxins, imbalance of metabolic homeostasis) as well from exogenous sources (i.e., pollutants, environmental chemical elements). There is relevant evidence that different minerals, such asbestos, quartz, amorphous silica, as well as alloys and nanoparticles, can be considered sterile stressors able to trigger a sterile inflammation by ATP imbalance, ROS production and increase of IL-1 cytokine family production (Rock et al., 2010). In particular, the IL-1 cytokine family displays a relevant role in triggering sterile inflammatory reactions which may ultimately evolve into a chronic state when the organism is unable to effectively fight the harmful agent (Rock et al., 2010; Lukens et al., 2012; Leso et al., 2018).

In conclusion, our study suggests that the direct contact with chrysotile, crocidolite and erionite, although to a different extent, induces the development of a sterile inflammatory pathway, due to the oxidative status of cells as well to the induction of cytokines and chemokines in the microenvironment where the mineral fibres are deposited causing a subtoxic cell damage. At the same time, we were able to highlight the different extent of naïve monocytes engagement and activation upon the indirect stimulus obtained by incubation with conditioned media from fibre treated alveolar epithelial and macrophage cells, demonstrating the higher indirect and direct inflammatory potential of chrysotile as compared to crocidolite and erionite. Finally, our results indicate that the common definition of chrysotile as the less toxic asbestos fibre, may be reconsidered, in order to prudently raise the alarm on its potential harmful effects on exposed subjects.

ACKNOWLEDGEMENTS

This research was conducted through funds from the project "Fibres: a multidisciplinary mineralogical, crystal-chemical and biological project to amend the paradigm of toxicity and carcinogenicity of mineral fibres" funded by the Italian Ministry of University and Research (PRIN-Bando 2017-Prot. 20173 × 8WA4).

REFERENCES

Ballirano P., Bloise A., Gualtieri A. F., Lezzerini M., Pacella A., Perchiazzi N., Dogan M., Dogan A. U., 2017. The crystal structure of mineral fibres. European Mineralogical Union Notes in Mineralogy 18, 17-64.

Barlow C.A., Grespin M., Best E.A., 2017. Asbestos fiber length and its relation to disease risk. Inhalation Toxicology 29, 541-554.

Baur X. and Frank A.L., 2021. Ongoing downplaying of the carcinogenicity of chrysotile asbestos by vested interests. Journal of Occupational Medicine and Toxicology 16, 1-10.

Bosshart H. and Heinzelmann M., 2016. THP-1 cells as a model for human monocytes. Annals of Translational Medicine 4(21), 438.

Cox L.A.Jr., 2018. Biological mechanisms of non-linear dose-response for respirable mineral fibers. Toxicology and applied pharmacology 361, 137-144.

Cox L.A.Jr., 2019. Dose-response modeling of NLRP3 inflammasome-mediated diseases: asbestos, lung cancer, and malignant mesothelioma as examples. Critical reviews in toxicology 49, 614-635.

Cox L.A.Jr., 2020. Nonlinear dose-time-response functions and health-protective exposure limits for inflammation-mediated diseases. Environmental research 182, 109026.

Croce A., Musa M., Allegrina M., Rinaudo C., Bariş Y.I., Dogan A.U., Powers A.A., Rivera Z.S., Bertino P., Yang H., Gaudino G., Carbone M., 2013. Micro-Raman spectroscopy identifies crocidolite and erionite fibers in tissue sections. Journal of Raman Spectroscopy 44, 1440-1445.

De La Fuente G., Fontana M., Asnaghi V., Chiantore M., Mirata S., Salis A., Damonte G., Scarfì S., 2020. The remarkable antioxidant and anti-inflammatory potential of the extracts of the brown alga Cystoseira amentacea var. stricta. Marine Drugs 19, 2.

Dikensoy O., 2008. Mesothelioma due to environmental exposure to erionite in Turkey. Current Opinion in Pulmonary Medicine 14, 322-325.

Dinarello C.A., 2018. Overview of the IL-1 family in innate inflammation and acquired immunity. Immunological reviews 281, 8-27.

Egilman D. and Howe S., 2007. Against Anti-health Epidemiology: Corporate Obstruction of Public Health via Manipulation of Epidemiology. International Journal of Occupational and Environmental Health 13, 118-124.

Epelman S., Lavine K.J., Randolph G.J., 2014. Origin and functions of tissue macrophages. Immunity 41, 21-35.

Fornasini L., Raneri S., Bersani D., Mantovani L., Scognamiglio V., Di Giuseppe D., Gualtieri A.F., 2022. Identification of iron compounds in chrysotile from the Balangero mine (Turin, Italy) by micro-Raman spectroscopy. Journal of Raman Spectroscopy 53, 1931-1941.

Gaudino G., Xue J., Yang H., 2020. How asbestos and other fibers cause mesothelioma. Translational lung cancer research 9(Suppl 1), S39-S46.

Giordani M., Mattioli M., Ballirano P., Pacella A., Cenni M., Boscardin M., Valentini L., 2017. Geological occurrence, mineralogical characterization, and risk assessment of potentially carcinogenic erionite in Italy. Journal of Toxicology and Environmental Health - Part B: Critical Reviews 20, 81-103.

Gualtieri A.F., 2021. Bridging the gap between toxicity and carcinogenicity of mineral fibres by connecting the fibre crystal-chemical and physical parameters to the key characteristics of cancer. Current Research in Toxicology 2, 42-52.

Gualtieri A.F., 2023. Journey to the centre of the lung. The perspective of a mineralogist on the carcinogenic effects of mineral fibres in the lungs. Journal of Hazardous Materials 442, 130077.

Gualtieri A.F., Gandolfi N.B., Pollastri S., Pollok K., Langenhorst F., 2016. Where is iron in erionite? A multidisciplinary study on fibrous erionite-Na from Jersey (Nevada, USA). Scientific Reports 6, 1-11.

Gualtieri A.F., Lusvardi G., Zoboli A., Di Giuseppe D., Lassinantti Gualtieri M., 2019. Biodurability and release of metals during the dissolution of chrysotile, crocidolite and fibrous erionite. Environmental Research 171, 550-557.

Gualtieri A.F., Pollastri S., Bursi Gandolfi N., Gualtieri M.L., 2018. In vitro acellular dissolution of mineral fibres: A comparative study. Scientific Reports 8, 1-12.

Guilliams M., Mildner A., Yona S., 2018. Developmental and Functional Heterogeneity of Monocytes. Immunity, 49, 595-613.

IARC Working Group on the Evaluation of Carcinogenic Risks to Humans, 2012. Arsenic, metals, fibres, and dusts. IARC monographs on the evaluation of carcinogenic risks to humans, 100(Pt C), 407-443.

Iles K.E. and Forman H.J., 2002. Macrophage signaling and respiratory burst. Immunologic Research 26, 95-105.

Leso V., Fontana L., Iavicoli I., 2018. Nanomaterial exposure and sterile inflammatory reactions. Toxicology and applied pharmacology 355, 80-92.

Li Y., Huang H., Liu B., Zhang Y., Pan X., Yu X.Y., Shen Z., Song Y.H., 2021. Inflammasomes as therapeutic targets in human diseases. Signal transduction and targeted therapy 6, 247.

Littlefield M.J., Teboul I., Voloshyna I., Reiss A.B., 2014. Polarization of Human THP-1 Macrophages: Link between Adenosine Receptors, Inflammation and Lipid Accumulation. International Journal of Immunology 1.

Lukens J.R., Gross J.M., Kanneganti T.D., 2012. IL-1 family cytokines trigger sterile inflammatory disease. Frontiers in Immunology 3, 315.

Madl A.K. and O'Neill H.C., 2023. Fiber biodurability and biopersistence: historical toxicological perspective of synthetic vitreous fibers (SVFs), the long fiber paradigm, and implications for advanced materials. Critical Reviews in Toxicology 52(10), 1-56.

Matés J.M., Segura J.A., Alonso F.J., Márquez J., 2008. Intracellular redox status and oxidative stress: implications for cell proliferation, apoptosis, and carcinogenesis. Archives of toxicology 82, 273-299.

Mattioli M., Giordani M., Dogan M., Cangiotti M., Avella G., Giorgi R., Dogan A.U., Ottaviani M.F., 2016. Morpho-chemical characterization and surface properties of carcinogenic zeolite fibers. Journal of Hazardous Materials 306, 140-148.

Mirata S., Almonti V., Di Giuseppe D., Fornasini L., Raneri S., Vernazza S., Bersani D., Gualtieri A.F., Bassi A.M., Scarfì S., 2022. The Acute Toxicity of Mineral Fibres: A Systematic In Vitro Study Using Different THP-1 Macrophage Phenotypes. International journal of molecular sciences 23, 2840.

Movia D., Bruni-Favier S., Prina-Mello A., 2020. In vitro Alternatives to Acute Inhalation Toxicity Studies in Animal Models-A Perspective. Frontiers in bioengineering and biotechnology 8, 549.

Müller L., Riediker M., Wick P., Mohr M., Gehr P., Rothen-Rutishauser B., 2010. Oxidative stress and inflammation response after nanoparticle exposure: differences between human lung cell monocultures and an advanced three-dimensional model of the human epithelial airways. Journal of The Royal Society Interface 7, S27-S40.

O'Reilly K.M., Mclaughlin A.M., Beckett W.S., Sime P.J., 2007. Asbestos-related lung disease. American family physician 75, 683-688.

Organization for Economic Co-operation and Development (OECD), 2009a. OECD guideline for the testing of chemicals. http://www.oecd.org/chemicalsafety/testing/oecdguidelinesforthetestingofchemicals.htm.

Organization for Economic Co-operation and Development (OECD), 2009b. Test No. 403: Acute Inhalation Toxicity. http://www.oecd.org/chemicalsafety/testing/oecdguidelinesforthetestingofchemicals.htm.

Organization for Economic Co-operation and Development (OECD), 2009c. Test No. 436: Acute Inhalation Toxicity-Acute Toxic Class Method. http://www.oecd.org/chemicalsafety/testing/oecdguidelinesforthetestingofchemicals.htm.

Organization for Economic Co-operation and Development (OECD), 2018. Guidance Document on Acute Inhalation Toxicity Testing. Series on Testing and Assessment, No. 39 (Second Edition). http://www.oecd.org/chemicalsafety/testing/oecdguidelinesforthetestingofchemicals.htm.

Pacella A., Andreozzi G.B., Nodari L., Ballirano P., 2019. Chemical and structural characterization of UICC crocidolite fibres from Koegas Mine, Northern Cape (South Africa). Periodico di Mineralogia 88, 297-306.

Petriglieri J.R., Salvioli-Mariani E., Mantovani L., Tribaudino M., Lottici P.P., Laporte-Magoni C., Bersani D., 2015. Micro-Raman mapping of the polymorphs of serpentine. Journal of Raman Spectroscopy 46, 953-958.

Pollastri S., Perchiazzi N., Lezzerini M., Plaisier J.R., Cavallo A., Dalconi M.C., Gandolfi N.B., Gualtieri A.F. 2016. The crystal structure of mineral fibres. 1. Chrysotile. Periodico di Mineralogia 85, 249-259.

Pozzolini M., Vergani L., Ragazzoni M., Delpiano L., Grasselli

E., Voci A., Giovine M., Scarfì S., 2016. Different reactivity of primary fibroblasts and endothelial cells towards crystalline silica: A surface radical matter. Toxicology 361-362, 12-23.

Rinaudo C., Belluso E., Gastaldi D., 2004. Assessment of the use of Raman spectroscopy for the determination of amphibole asbestos. Mineralogical Magazine 68, 455-465.

Rock K.L., Latz E., Ontiveros F., Kono H., 2010. The sterile inflammatory response. Annual review of immunology 28, 321-342.

Smith M.T., Guyton K.Z., Gibbons C.F., Fritz J.M., Portier C.J., Rusyn I., DeMarini D.M., Caldwell J.C., Kavlock R.J., Lambert P.F., Hecht S.S., Bucher J.R., Stewart B.W., Baan R.A., Cogliano V.J., Straif K., 2016. Key Characteristics of Carcinogens as a Basis for Organizing Data on Mechanisms of Carcinogenesis. Environmental Health Perspectives 124, 713-21.

Tsai Y.-L., Huang E., Li Y.-H., Hung H.-T., Jiang J.-H., Liu T.-C., Fang J.-N., Chen H.-F., 2021. Raman spectroscopic characteristics of zeolite group minerals. Minerals 11, 167.

Vandesompele J., De Preter K., Pattyn F., Poppe B., Van Roy N., De Paepe A., Speleman F., 2002. Accurate normalization of real-time quantitative RT-PCR data by geometric averaging of multiple internal control genes. Genome biology 3(7), RESEARCH0034.

Weber A., Wasiliew P., Kracht M., 2010. Interleukin-1 (IL-1) pathway. Science signaling 3(105), cm1.

Yu S., Choi H.-H., Kim I. W., Kim, T.-J., 2019. Conditioned medium from asbestos-exposed fibroblasts affects proliferation and invasion of lung cancer cell lines. PLOS ONE 14(9), e0222160.

Zelová H. and Hošek J., 2013. TNF-α signalling and inflammation: interactions between old acquaintances. Inflammation Research 62, 641-651.

Zhou D.R., Eid R., Miller K.A., Boucher E., Mandato C.A., Greenwood M.T., 2019. Intracellular second messengers mediate stress inducible hormesis and Programmed Cell Death: A review. Biochimica et biophysica acta. Molecular Cell Research 1866, 773-792.